AGU PUBLICATIONS

JGR

Journal of Geophysical Research: Space Physics

RESEARCH ARTICLE
10.1002/2015JA022217

Special Section:
Energetic Electron Loss and its Impacts on the Atmosphere

Nighttime mesospheric hydroxyl enhancements during SEP events and accompanying geomagnetic storms: Ionization rate modeling and Aura satellite observations

O. P. Verkhoglyadova[1,2], J. M. Wissing[3], S. Wang[1], M.-B. Kallenrode[3], and G. P. Zank[2,4]

[1]Jet Propulsion Laboratory, California Institute of Technology, Pasadena, California, USA, [2]Department of Space Science, University of Alabama in Huntsville, Huntsville, Alabama, USA, [3]Institute of Environmental Systems Research, University of Osnabrück, Osnabrück, Germany, [4]Center for Space and Aeronomic Research, University of Alabama in Huntsville, Huntsville, Alabama, USA

Key Points:
- Mesosphere ionization rates with realistic particle precipitation inputs are modeled during two SEP events and concomitant magnetic storms
- Results are consistent with nighttime odd hydrogen density enhancements observed by Aura
- Combined precipitating populations of SEPs and magnetospheric electrons are important for mesospheric ionization chemistry

Correspondence to:
O. P. Verkhoglyadova,
Olga.Verkhoglyadova@jpl.nasa.gov

Citation:
Verkhoglyadova, O. P., J. M. Wissing, S. Wang, M.-B. Kallenrode, and G. P. Zank (2016), Nighttime mesospheric hydroxyl enhancements during SEP events and accompanying geomagnetic storms: Ionization rate modeling and Aura satellite observations, *J. Geophys. Res. Space Physics*, *121*, 6017–6030, doi:10.1002/2015JA022217.

Received 30 NOV 2015
Accepted 15 JUN 2016
Accepted article online 18 JUN 2016
Published online 5 JUL 2016

Abstract We quantify the effects of combined precipitating solar protons and magnetospheric electrons on nighttime odd hydrogen density enhancements during two solar energetic particle (SEP) events accompanied by strong geomagnetic storms. We perform detailed modeling of ionization rates for 7–17 November 2004 and 20–30 August 2005 intervals with improved version 1.6 of the Atmospheric Ionization Module Osnabrück model. Particle measurements from Geostationary Operational Environmental Satellites and Polar Orbiting Environmental Satellites are sorted and combined in 2 h intervals to create realistic particle precipitation maps that are used as the modeling input. We show that modeled atmospheric ionization rates and estimated peak odd hydrogen (primarily hydroxyl) production from 0.001 hPa to 0.1 hPa atmospheric pressure levels during these intervals are consistent with enhancements in nighttime averaged zonal odd hydrogen densities derived from newly reprocessed and improved data set of Microwave Limb Sounder instrument on board Aura satellite. We show that both precipitating SEPs and magnetospheric electrons contribute to mesospheric ionization and their relative contributions change throughout the intervals. Our event-based modeling results underline the importance of the combined ionization sources for odd hydrogen chemistry in the middle atmosphere.

1. Introduction

Solar energetic particles (SEPs) in interplanetary space originate from solar flares or result from seed particle acceleration (protons having the largest fluxes) at interplanetary shocks driven by coronal mass ejections (CMEs) [e.g., *Cane et al*., 1988; *Kallenrode*, 2003; *Zank et al*., 2007; *Verkhoglyadova et al*., 2014]. Earth-directed SEPs can penetrate into the Earth magnetosphere and high-latitude neutral atmosphere to the lowest altitude determined by the particle energy. SEPs are known to affect middle atmosphere (mesosphere and upper stratosphere) chemistry. The main mechanism is through ionization by precipitating high-energy particles, e.g., protons with ~5 MeV deposit their maximum energy at ~75 km altitude, which leads to an efficient ionization of atmosphere at this altitude [*Turunen et al*., 2009; *Wissing and Kallenrode*, 2009]. Among other effects, SEPs create odd hydrogen (HO_x, primarily hydroxyl OH and HO_2) species through ion chemistry and cause ozone (O_3) destruction in the mesosphere [*Solomon et al*., 1981, 1983; *Jackman et al*., 2005, 2006, 2011; *Verronen et al*., 2006, 2007; *Damiani et al*., 2008, 2010; *Verkhoglyadova et al*., 2015]. For example, tertiary ozone maximum observed in wintertime high-latitude mesosphere around that altitude range [*Marsh et al*., 2001] is strongly affected by SEPs [*Seppälä et al*., 2006; *Sofieva et al*., 2009].

If a CME causes a geomagnetic storm, disturbances in the Earth magnetosphere allow SEPs of certain energies to penetrate down to latitudes that are lower than cutoff latitudes in the absence of a storm [*Leske et al*., 2001; *Verronen et al*., 2007]. *Leske et al*. [2001] found a correspondence between the lowest latitude for energetic proton penetration and the level of geomagnetic activity. They showed that protons can penetrate down to 55° latitude during the main phase of a large geomagnetic storm. Modeling over the time scale of 200 years confirmed that the weakening of the Earth's magnetic field (unrelated to geomagnetic storms) could lead to a decrease in shielding, an increase in precipitating solar proton flux, and ozone destruction due to ion chemistry reactions involving OH and other species [*Winkler et al*., 2008]. In this

paper we will analyze ionization of the mesosphere from 70° (auroral) to 50° (subauroral) geographic latitudes in both hemispheres.

In our previous paper [*Verkhoglyadova et al*., 2015, hereafter Paper I] we reported observations of changes in nighttime hydroxyl and ozone during two SEP events of 7–17 November 2004 and 20–30 August 2005 based on global measurements by two satellites. We showed a correspondence between the energetic proton flux (>10 MeV) measured at the Earth's orbit and the nighttime zonal average OH partial column density enhancements between 0.005 and 0.1 hPa (approximately from 65 km to 85 km in altitude). If observed enhancement in nighttime OH density is created through the ionization of the mesosphere by SEPs, it should directly depend on mesosphere ionization rates in the course of the SEP event. In this paper we use the Atmospheric Ionization Module Osnabrück (AIMOS) model [*Wissing and Kallenrode*, 2009] (described in section 3.1) to calculate atmospheric ionization rates for measured energetic solar proton fluxes and estimate corresponding changes in OH abundance. We focus on energetic solar protons and ignore the contribution from other ion species of SEPs. However, this is only one factor contributing to OH enhancement.

Both SEP events were associated with strong CME-driven storms. It was shown by *Verronen et al*. [2011] that energetic magnetospheric electrons precipitating into the middle atmosphere from the Earth radiation belts during geomagnetic storms can cause OH enhancements. *Andersson et al*. [2012] performed a detailed analysis of magnetospheric electron precipitation that causes OH enhancements and showed a strong correlation between mesospheric OH mixing ratios and electron count rates. Electrons of lower energies than protons precipitate at the same altitude. For instance, electrons with energies ~1 MeV and protons with energies ~20 MeV deposit their maximum energy at ~60 km altitude. Results of Paper I indicate that electrons can have an important contribution to OH density increases for the analyzed events, especially during the November 2004 interval.

Effects of precipitating solar protons and magnetospheric electrons on middle atmospheric hydroxyl have been modeled separately, and an agreement between observations and modeling has been demonstrated [see, e.g., *Jackman et al*., 2005; *Verronen et al*., 2013]. The study by *Funke et al*. [2011] analyzed composition changes in middle atmosphere (not including OH) following the Halloween event of October 2003, due to ionization by both protons and electrons calculated with the AIMOS model. AIMOS (http://aimos.physik.uos.de) calculates atmospheric ion pair production rates based on data from the Polar Orbiting Environmental Satellites (POES) and the Geostationary Operational Environmental Satellites (GOES). The combination of long-term observations from several satellites and a special sorting algorithm allows for a high-resolution spatial precipitation pattern. The wide energy range (154 eV to 500 MeV for protons and 154 eV to 300 keV for electrons) covers the majority of the SEP fluxes and magnetospheric electron fluxes, and the model calculates ionization rate profiles on a 2 h basis [*Wissing and Kallenrode*, 2009] (see section 3.1 for details).

The modeling approach by *Funke et al*. [2011] is based on AIMOS version 1.2 which had several issues with calculated electron ionization rate. Uncertainty in upper energy threshold of an electron channel of POES particle detector affected calculation of electron-induced ionization rates below ~70 km and resulted in overestimation of ionization between 50 and 70 km. Another cause for overestimation of electron ionization below 90 km is contamination in the electron detector by high energetic proton flux. *Verronen et al*. [2015] in their study of proton and electron precipitation effects during SEPs and strong storms indicate that the use of AIMOS v.1.2 resulted in only about 50% agreement with observed electron density. Both papers state that the electron detector issue affected their results. In this paper, we use the revised AIMOS version 1.6, which neglects the problematic electron channel and filters the remaining electron channels during periods of high proton flux. Thus, we can expect more realistic electron ionization rates between 70 and 90 km. For altitudes below 70 km AIMOS cannot provide electron-induced ionization rates.

In this study we use a combined modeling approach by including both precipitating protons and electrons into improved AIMOS model with more realistic forcing. To our knowledge, this is the first modeling study of hydroxyl enhancements which utilizes the combined precipitation input. To utilize realistic model inputs, we retrieve, sort, and combine electron and proton spectra in a broad energy range from in situ satellite measurements. These data are used to create precipitation maps with 2 h temporal resolution. This modeling approach allows for a comparison of the relative contributions of different particle populations to atmospheric ionization rates throughout SEP events and concomitant geomagnetic storms. The SEP events

analyzed in this paper are moderate events, and we expect comparable solar proton and magnetospheric electron contributions to middle atmospheric ionization.

The goal of our study is to quantitatively connect precipitating solar protons and magnetospheric electrons with cumulative ionization rates and nighttime mesospheric OH density enhancements to provide better understanding of how the combined effect controls OH abundance during SEP events and concomitant geomagnetic storms. Following our previous study of the November 2004 and August 2005 events, we perform a more detailed analysis of a connection between atmospheric effects and precipitating particle fluxes in a certain energy range corresponding to the maximum energy release at altitudes where OH enhancements are observed.

The paper has the following structure. We begin with a brief summary of satellite observations of OH, SEPs, and geomagnetic conditions during two SEP events. Then we describe the modeling approach, input parameters based on energetic proton, and electron fluxes derived from satellite observations. Then we present the main results on calculating mesosphere ionization rates and hydroxyl production. The paper will conclude with discussions of a correspondence between the modeled rates and observed nighttime OH density enhancements and quantification of the results.

2. Brief Overview of Aura/MLS Observations of Nighttime OH Abundances During Two SEP Events

The Aura satellite is one element of the NASA Earth observing satellites at a near-Earth orbit. The Microwave Limb Sounder (MLS) instrument on board Aura provides global measurements of HO_x species by scanning the Earth's stratosphere and mesosphere from near the surface to about 90 km altitude every ~25 s and generates about 3495 vertical profiles for each species on a daily basis [*Waters et al*., 2006; *Pickett et al*., 2006a, 2006b; *Livesey et al*., 2006]. Paper I studied middle atmosphere effects of two SEP events that occurred during the periods of 7–17 November 2004 and 20–30 August 2005, with the main phases of the SEP events on 7–10 November 2004 (double SEP event) and 23–24 August 2005, respectively. Among other results, Paper I analyzed the averaged nighttime OH partial column density in the pressure range from 0.005 to 0.2 hPa, which corresponds approximately to the altitude range of 65–80 km. Whereas Paper I used MLS v3.3 data, in our present study, we use OH data from the recently released new version v4.2 with improvements in the mesospheric OH data quality [*Livesey et al*., 2015]. The overly tight a priori constraints in previous versions, which causes data near the mesospheric OH density peak (~0.032 hPa) in the summer hemisphere (or tropics when near the equinox) to be strongly influenced by a priori information, are fixed in the new version. Also, the smaller bias at 10–15 hPa in v4.2 eliminates the need of day-night correction for bias for the corresponding data. However, there are sometimes zig-zags in v4.2 nighttime mesospheric OH vertical profiles, which is a side effect of fixing the possible positive bias introduced by tight lower limits set in previous version retrievals.

We focus on nighttime measurements with the solar zenith angle (SZA) $>95°$ because of higher uncertainties in analyzing SEP-related signatures during daytime conditions (since a larger background density of odd hydrogen species is produced by solar UV radiation). With a Sun-synchronized orbit, the MLS overpass time at low to middle latitudes varies very little from night to night. At high latitudes (especially above 70°) during polar night, however, the local solar time of MLS measurements has a much wider spread. To better present data for these cases, two zonal average OH values are calculated for each night. Each point has its own average "date" calculated based on the average local solar time of the measurements and expressed as a fraction of the corresponding calendar day.

Figure 1 shows a time series of zonal-averaged vertical profiles of OH density for two SEP events derived from Aura/MLS measurements. Measurements are presented in the pressure range from 0.001 hPa to 0.1 hPa and in high-latitude bins only. Figures 1a–1ad show the nighttime zonal average OH density for the November event in four latitude bins, [60°, 70°], [50°, 60°], [−60°, −50°], and [−70°, −60°]. The time interval of the SEP event is shown by red vertical lines. Enhancements in OH density occur during the SEP interval. There is an enhancement observed at a later time from 10 November and outside of the SEP interval. This enhancement is discussed below. Figures 1e−1h show OH enhancements in four latitude bins during the August 2005 event. The SEP event is shorter (shown by the red vertical lines) with the largest SEP-related enhancement in nighttime zonal average OH density being observed in the [60°, 70°] latitude bin. Horizontal stripes seen

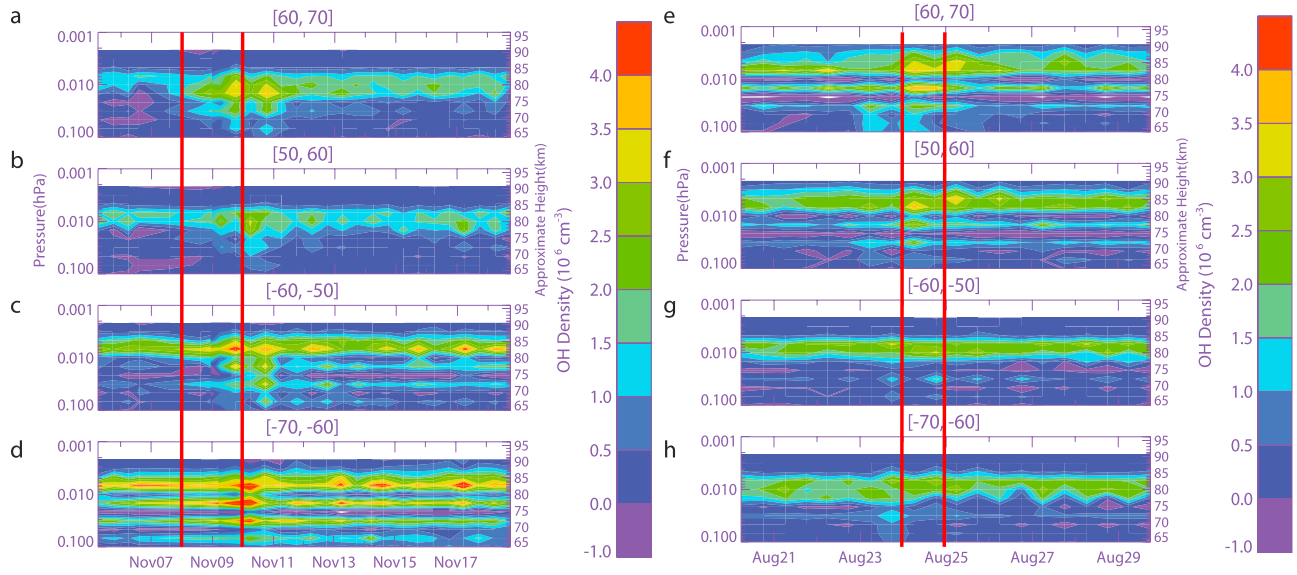

Figure 1. Aura/MLS daily averaged zonal vertical profiles of OH density for the (a–d) November 2004 and (e–h) August 2005 SEP event intervals during local nighttime (SZA > 95°). Data are binned in several latitude bins: [60°, 70°], [50°, 60°], [−60°, −50°], and [−70°, −60°]. Middle-atmosphere pressure range from 0.001 hPa to 0.1 hPa only is shown. Approximate intervals of SEP events are shown by red vertical lines.

in Figures 1c−1f are not real. This is a side effect of fixing the possible positive bias in nighttime mesospheric OH vertical profiles introduced by tight lower limits set in previous version retrievals (see *Livesey et al*. [2015] for discussion on MLS v4.2 data quality).

Both SEP events were associated with flares, CMEs, and strong geomagnetic storms with peak intensities of ~−393 nT and ~−174 nT for the November and August events, respectively. Figure 2 shows the 5 min averaged *SYM-H* index during two events which reflect the evolution of the magnetospheric ring current and the dynamics of a geomagnetic storm [*Iyemori*, 1990]. Disturbed geomagnetic conditions led to solar proton penetration down to ~50° to 60° latitudes, which corresponds to nighttime localized OH density enhancements (see Figures 1b, 1c, 1f, and 1g and Paper I). *Wissing et al*. [2008] have found an equatorward expansion

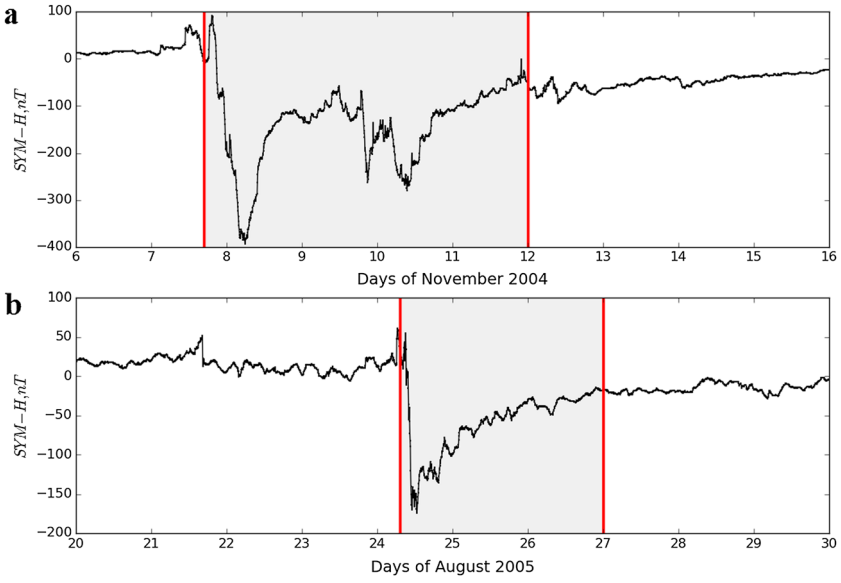

Figure 2. Geomagnetic activity index *SYM-H* during the (a) November 2004 and (b) August 2005 intervals. Vertical red lines indicate approximate time range of geomagnetic storms.

of auroral particle precipitation in accordance with geomagnetic activity level. Both mechanisms, i.e., SEPs and auroral electrons, could contribute to equatorward spreading of OH enhancements.

3. Modeling of Mesospheric Ionization Due To Energetic Particle Precipitation

We apply the AIMOS to model ion pair production rates due to precipitating protons and electrons to quantify the effect of SEP events and concomitant geomagnetic storms on mesosphere ion chemistry.

3.1. Brief Description of AIMOS Modeling Approach

The AIMOS model [*Wissing and Kallenrode*, 2009] has been developed to provide 3-D particle ionization rates for climate modeling. The main components are as follows: a sorting algorithm that determines the particle flux at any given position on top of the atmosphere and a Monte Carlo model that calculates the energy deposition (ionization) of the particle flux inside the atmosphere.

The challenge in establishing a spatial particle precipitation pattern is the limited availability of measurements. Even though the AIMOS model uses measurements from three different satellites, only two of them provide spatially resolved data, the POES satellites, covering the track below the polar orbit by point measurements in about 90 min. This defines the minimal temporal resolution of the model which has been set to 2 h. Since the particle flux is highly variable (spatially about 3 orders of magnitude in one orbit and even more for a particular location during an SEP), AIMOS attempts to generate long-term mean precipitation maps on a 3.75° by 3.75° grid sorted by geomagnetic disturbance. The result is a 2-D precipitation pattern that clearly reflects the equatorward movement of the precipitating magnetospheric flux with increasing K_p storm index. These precipitation maps provide spatial patterns only, and in AIMOS they are scaled by satellite flux observations to obtain temporal record of ionization in 2 h resolution. In a second step, data from the high-energy GOES channels are used for the polar cap area together with the second highest-energy POES proton channel (mep0P4). Finally, the sorting algorithm produces electron, proton, and alpha spectra fits for every grid point. Specifically, we use up to five power law functions with variable intersections.

The calculation of the ionization rate is done by a Monte Carlo model based on Geant4 [*Agostinelli et al*., 2003]. This model represents the Earth's atmosphere divided into 67 logarithmically equidistant pressure levels and allows to simulate the energy deposition by energetic particles. The atmospheric composition originates from a 10 year reference run of the HAMMONIA climate model [*Schmidt et al*., 2006] with an upper altitude boundary above 250 km.

The effective altitude range of AIMOS is restricted to available (and reliable) particle measurements. For electrons, the energy extends from 154 eV to 300 keV, resulting in an altitude range of 70–250 km. For protons, the measurements range from 154 eV up to 500 MeV energies and yield a range of 16–250 km. Alpha particles are not considered in this paper. To study the impact of ionization at different latitudes and to compare with MLS measurements, the gridded model output was sorted into four latitude bins, [60°, 70°], [50°, 60°], [−60°, −50°], and [−70°, −60°].

3.2. Model Input for Precipitating Particles

Figure 3 shows precipitating proton and electron fluxes in selected energy ranges as calculated from the AIMOS sorting algorithm for different latitude bins for the November 2004 event. Particle precipitation fluxes for the August 2005 event are shown in Figure 4. Different panels correspond to different latitude ranges. We focus on precipitating protons with energies between 0.8 MeV and 6.9 MeV and precipitating electrons with energies between 30 keV and 300 keV, which deposit their maximum energy in the altitude range of ~70 km to 95 km [*Wissing and Kallenrode*, 2009], i.e., where the density of mesospheric hydroxyl peaks. Since the proton detector sensitivity threshold is relatively high, the flux sometimes drops to zero during quieter times and especially in lower latitudes that are less affected by particle precipitation. Due to using a logarithmic graph, these periods are left blank. Energetic electron measurements during high activity periods show cautions (identified by red dots) due to possible contamination of the electron detectors by high-energy protons. In that case the possibly contaminated grid points are excluded, but not all subareas in the latitude bands will be affected by this contamination, only those regions that are in the proton precipitation zones. Thus, there is a chance of underestimating the electron precipitation fluxes at the high-energy end of the electron spectrum and the resulting local ionization due to precipitating electrons.

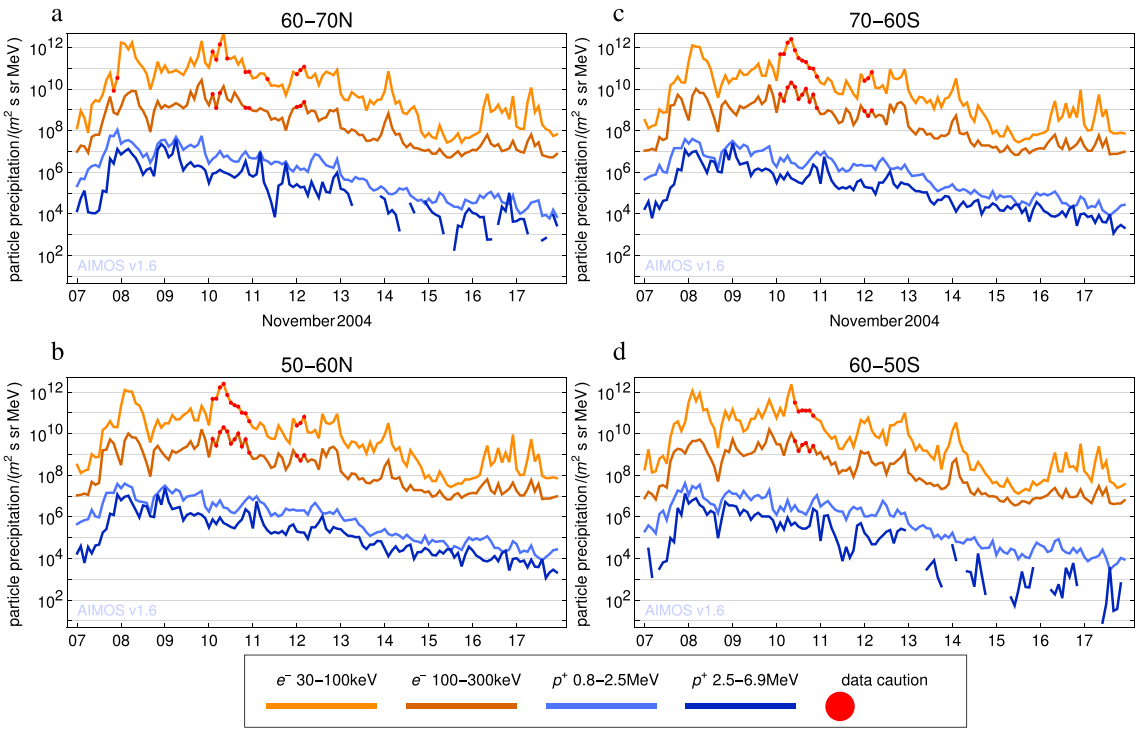

Figure 3. Precipitating particle fluxes as derived from the AIMOS sorting algorithm and used for the November 2004 event. Shown are the latitude ranges: (a) [60°, 70°], (b) [50°, 60°], (c) [−70°, −60°], and (d) [−60°, −50°]. Selected energy ranges for precipitating protons and electrons are shown in different colors. Data caution is sometimes noted for electron flux data. See text for details.

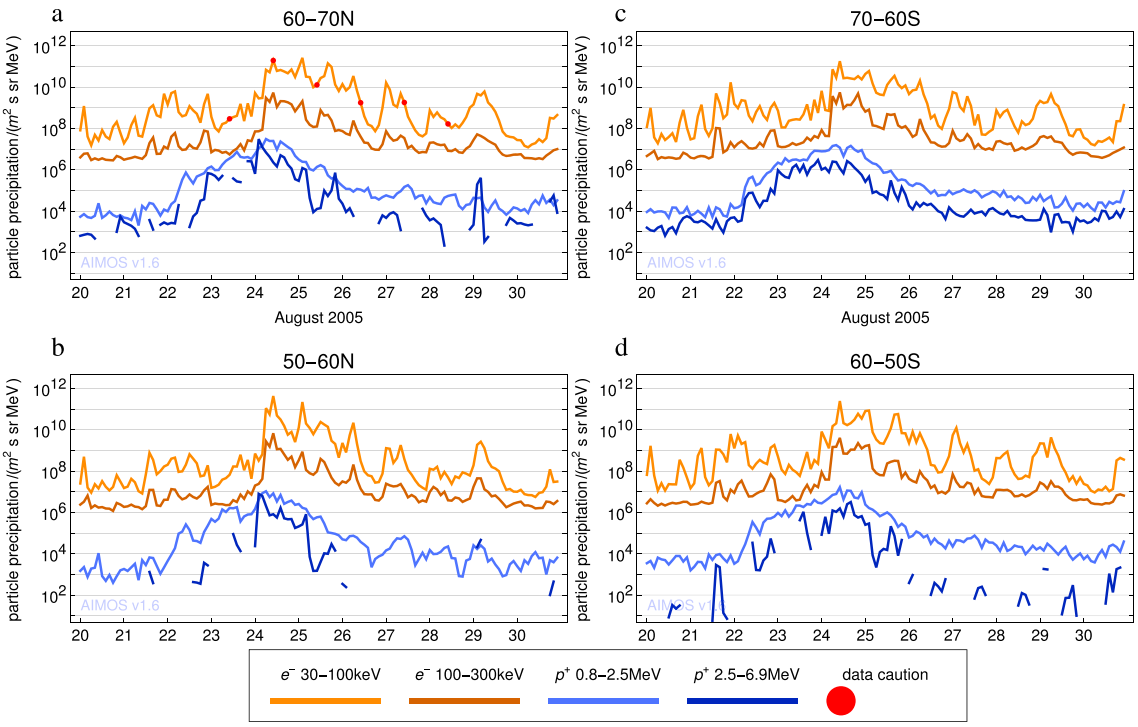

Figure 4. Precipitating particle fluxes as derived from the AIMOS sorting algorithm and used for processing the spatial resolved ionization rates for the August 2005 event. Shown are the latitude ranges: (a) [60°, 70°], (b) [50°, 60°], (c) [−70°, −60°], and (d) [−60°, −50°]. Selected energy ranges for precipitating protons and electrons are shown in different colors. Data caution is sometimes noted for electron flux data. See text for details.

Figure 3 shows that fluxes of precipitating protons (shown by blue lines) within selected energy ranges exhibit two peaks on 8 and 9 November (extended through 10 November). Proton fluxes are lower in magnitude than electron fluxes (shown by brown lines). Fluxes are about an order of magnitude lower for the lower latitudes (Figures 3b and 3d) as compared to the high latitudes (Figures 3a and 3c). The proton energy is ~25 times higher, which means that the electron impact on ionization is dominant. However, the altitude range on which the particle energy is deposited and mean ionization profile of protons and electrons are different. Thus, this difference in the number of fluxes between protons and electrons does not imply a similar difference in atmospheric impacts.

Precipitating electron fluxes peak on 8 November (shifted to a later time relative to the proton peak) and 10 November. Magnitudes and dynamics of electron fluxes are approximately the same in the different latitude ranges in both hemispheres. This also applies to proton fluxes.

Peaks in proton (or SEP) fluxes could be caused by X-class solar flares that occurred on 8 and 10 November, as well as by particles accelerated by CME-driven shocks. GOES-11 measurements of protons from 600 keV to ~150 MeV show SEP peaks on 8–10 November (see Paper I). Figure 2a shows that the main phase of the storm occurred at the beginning of 8 November with two additional enhancements in the ring current at the end of 9 November and at the beginning of 10 November. The geomagnetic activity is probably caused by a double CME (Paper I, Figure 1d). Interestingly, two electron channels in Figure 3 show peaks on the same days which could be due to precipitation of magnetospheric electrons during the geomagnetic storm.

Figure 4 shows that precipitating proton fluxes peak on 23–25 August and there is an isolated peak on 29 August. GOES-12 observations show multiple flares occurring on 22–24 August (Paper I, Figure 7) which possibly generated SEPs. CME-accelerated electrons possibly contribute to the total proton flux from 24 to approximately 26 August. According to the geomagnetic storm dynamics for the August 2005 event (Figure 2b), the storm main phase occurred on 24 August and was followed by a recovery phase. Precipitating electron fluxes (Figure 4) peak on 24–26 August (shifted to a later time relative to the peaks in proton fluxes) and have an isolated peak on 29 August. We present modeling results for ionization rates in the next section.

3.3. November 2004 SEP Event

We model the proton and electron ionization rates for the period of the November 2004 event, focusing on altitudes corresponding to the mesospheric pressure range from 0.001 hPa to 0.1 hPa. For the purpose of comparing modeled zonal mean ion pair production rates with local nighttime (LT) Aura/MLS observations (SZA $>$ 95°), we select the model data within a time window around the nightly zonal mean LT of a MLS measurement estimated for each latitude bin. Note that the actual instrument scan time for each signal vertical profile is different and the nighttime range of the actual measurement time varies with latitude. We select a ±1 h window around the nightly average LT of the MLS measurement for each latitude bin to account for temporal dynamics of OH enhancements. The lifetime of nighttime OH is of order of minutes, but a density enhancement due to SEPs could last hours or longer. Duration of the enhancement depends largely on the change of the ionization rates induced by energetic particles throughout the night. Figures 5a–5d show zonal mean ion pair production rates due to precipitating energetic protons for nighttime LTs. Latitude ranges for the zonal means are shown on top of the panels.

Figures 5a–5d show two main enhancements in zonal averaged ion production rates during the SEP event. The first enhancement occurred at the end of 7 November and at the beginning of 8 November. The second and lesser in magnitude enhancement occurred at the end of 8 November and at the beginning of 9 November, which extended through 10 November. If we compare with Figure 3, these enhancements coincide in time with peaks in energetic proton fluxes in the selected energy ranges. Based on particle precipitation data and modeling results, energetic protons contribute to the ionization of the nighttime mesosphere during these time intervals.

Figures 5a–5d indicate that most of the ionization during the nighttime occurred at high latitudes. There is an interhemispheric asymmetry with nighttime ionization enhancement spreading northward from −70° down to −50° and much less ionization estimated around 50°. Note that we calculated zonal averages in geographic coordinates rather than in geomagnetic coordinates. On one hand, this asymmetry could be an effect of a difference in geographic and magnetic latitude binning and the location difference of magnetic poles

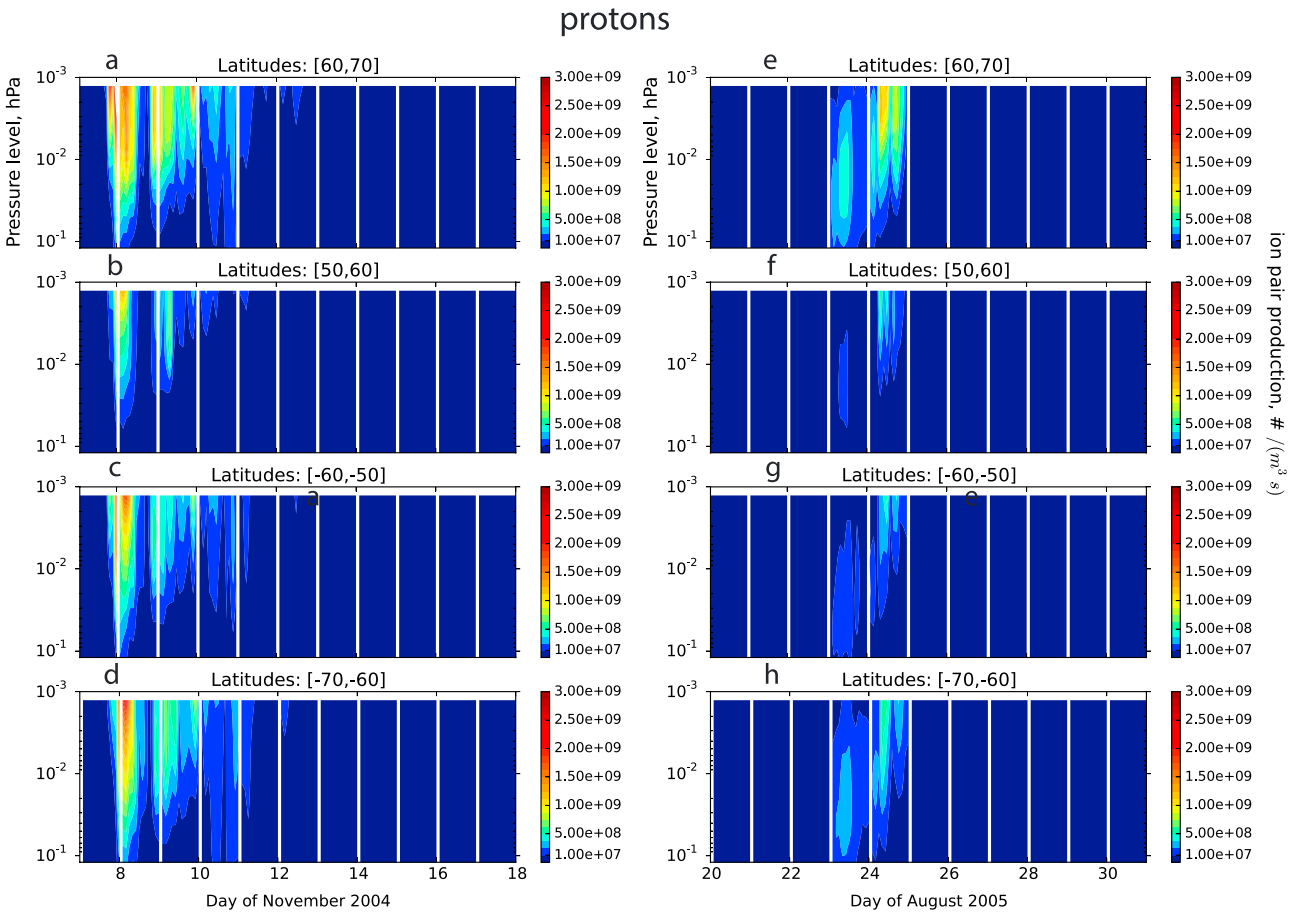

Figure 5. Zonal ion pair production rates due to atmosphere ionization by precipitating protons for the (a–d) November 2004 and (e–h) August 2005 intervals for the local time ranges (2 h window) corresponding to the average local time of MLS nighttime measurements (see text for details). Panels correspond to the latitude bins: [60°, 70°], [50°, 60°], [−60°, −50°], and [−70°, −60°]. Middle-atmosphere pressure range from 0.001 hPa to 0.1 hPa is shown.

relative to the geographic poles. While the magnetic northern pole in 2004 was located around ~82.8 N, the magnetic southern pole was located around ~64.6°S (from the NOAA model, http://www.ngdc.noaa.gov/geomag/GeomagneticPoles.shtml). Since the Earth's magnetic field configuration determines the precipitation zones, this shift may be the reason for a larger precipitation in the northern polar region (and less precipitation at 50–60 N).

On the other hand, enhancement in the Northern Hemisphere is not necessarily weaker if we consider the duration of the hemispheric responses (enhanced ionization in the northern polar hemisphere lasts longer than in the southern polar hemisphere). This result is in direct agreement with the observed asymmetry (in geographic coordinates) and features of zonal nighttime OH density enhancements throughout the SEP event (see a discussion in Paper I and Figure 1). Notice the increases in the OH density seen in the polar atmosphere on 8–10 November.

Figures 6a–6d show nighttime zonal averaged ionization rates due to precipitating electrons. The enhancement on 8 November coincides in time with the enhanced ionization due to energetic protons. The ionization due to electrons is comparable to that of protons, and both could significantly contribute to the observed OH enhancement. Notice the enhancement in ionization due to electrons on 10 November. It may cause a prolonged increase of OH through 10–11 November, as shown in Figures 1c and 1d. We will discuss physical mechanisms behind this effect in section 4.

3.4. August 2005 SEP Event

Model results of proton and electron ionization rates for the August 2005 SEP event are shown in Figures 5e–5h and 6e–6h. Figures 5e–5h shows that the main enhancement in daily averaged zonal ion production rates

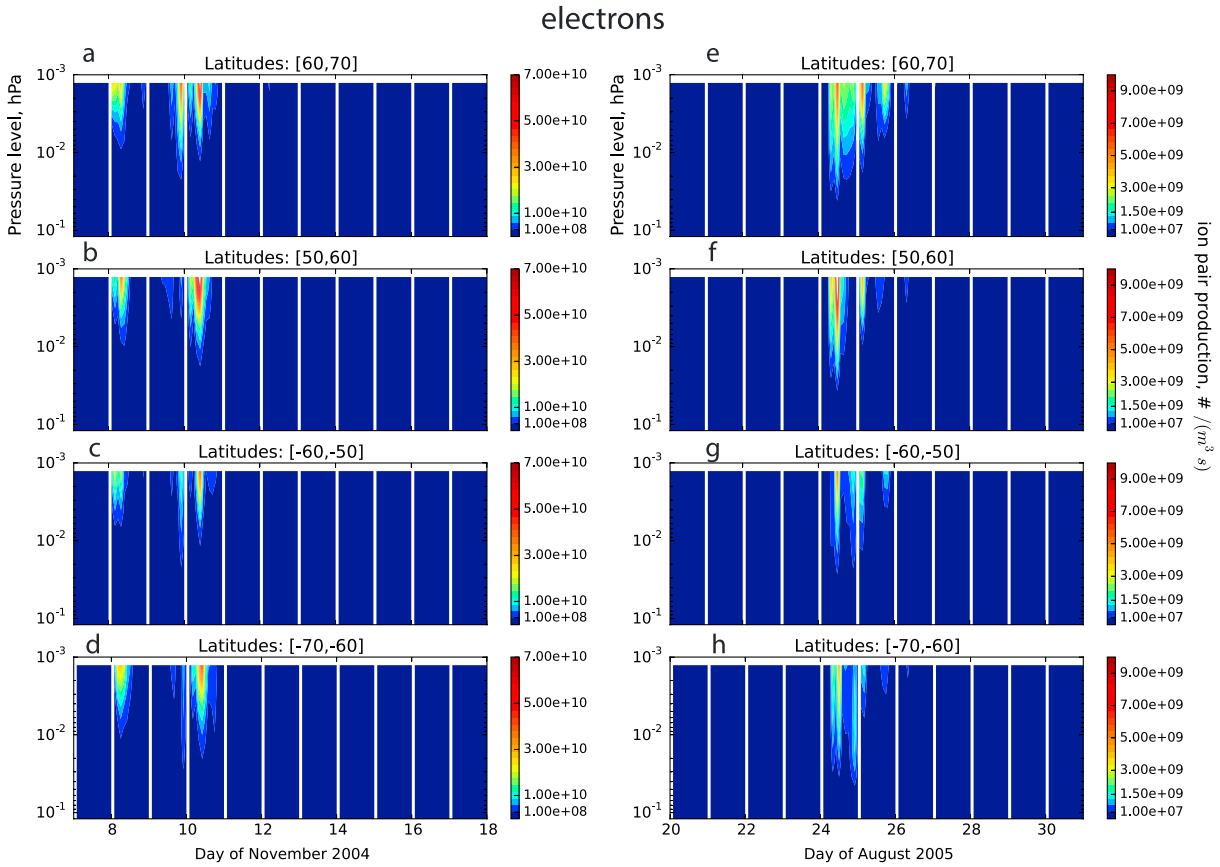

Figure 6. Zonal ion pair production rates due to atmosphere ionization by precipitating electrons for the (a–d) November 2004 and (e–h) August 2005 intervals for the local time ranges (2 h window) corresponding to the average local time of MLS nighttime measurements (see text for details). Panels correspond to the latitude bins: [60°, 70°], [50°, 60°], [−60°, −50°], and [−70°, −60°]. Middle-atmosphere pressure range from 0.001 hPa to 0.1 hPa is shown.

occurred at the beginning of 24 August with a weak enhancement preceding it on 23 August. The enhancements are more pronounced at polar latitudes (Figures 5e and 5h), and stronger ion production occurred in the Northern Hemisphere. However, this interhemispheric asymmetry could be due to a difference in binning in geographic and geomagnetic coordinates mentioned above. The largest enhancement coincides in time with the peaks in energetic proton fluxes at the selected energy range (see Figure 4). Figures 6e–6h show modeled nighttime zonal averaged ionization rates due to precipitating electrons. There is an enhancement on 24–25 August with two peaks. If we compare with Figure 2b, the largest enhancement coincides in time with a main and recovery phases of the geomagnetic storm. As for the previous case, ionization rates due to protons and electrons are comparable, but timings of peaks can be different. Enhancement in OH ends on 26 August (Figures 1e and 1f).

The November event is a stronger event in terms of the rate of ionization by both protons and electrons. Indeed, the fluxes reach higher values and stay elevated longer for the November event compared to the August event (compare left and right columns in Figures 5 and 6). The relative enhancement of electron fluxes could be explained by a stronger November storm (compare minimum values of *SYM-H* and storm main phase durations from Figure 2). Flares and double CMEs during the November event produced higher proton fluxes at >5 MeV energies than flares and a CME during the August event (Paper I, Figures 1, 7, and 11).

3.5. Relative Effects of Precipitating Protons and Electrons

We would like to clarify the role of precipitating protons and electrons for the middle atmosphere ionization in these events. The fraction of the ionization rate due to precipitating electrons versus altitude within

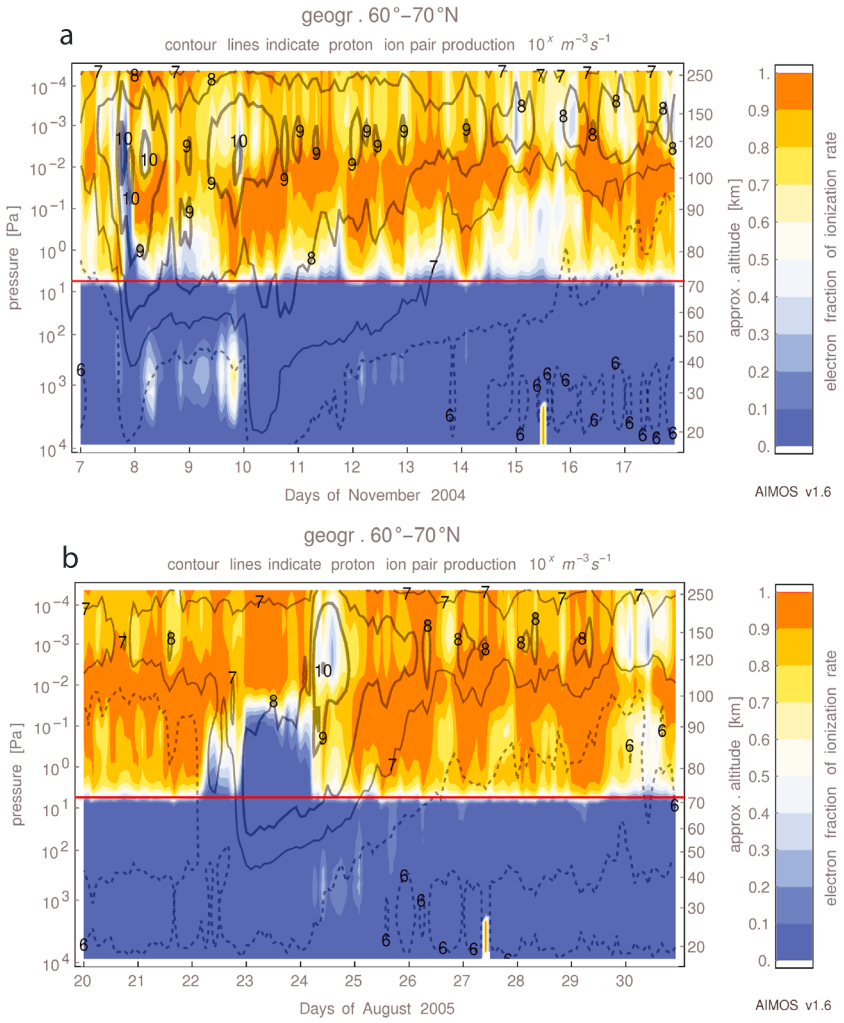

Figure 7. Fraction of ionization rate in the [60°, 70°] latitude bin due to precipitating auroral electrons for (a) the November 2004 event and (b) the August 2005 event obtained with the AIMOS. Contour lines indicate proton ion pair production in the orders of 10^x m^{-3} s^{-1}. Dashed, thin solid and thick solid lines correspond to the contours of 10^6 m^{-3} s^{-1}, 10^7 m^{-3} s^{-1}, and 10^8 m^{-3} s^{-1}, correspondingly. Results are shown for all local times. Red line drawn at about 70 km indicates the lowest altitude that is affected by direct ionization due to electrons.

[60°, 70°] latitude bin is estimated with the AIMOS 1.6. No separation for local time was done; i.e., the estimates are made for daytime and nighttime. Figure 7 shows the electron fraction of the ionization rates (shown in color) overplotted on the proton pair production rate (shown by contours). Ionization due to electrons with energies above 300 keV is not modeled. Red line drawn at about 70 km indicates the lowest altitude that is affected by direct ionization due to electrons. There is some ionization due to bremsstrahlung at lower altitudes. Since the model takes observations of protons with energies up to 500 MeV as input, ionization by a lower energy portion of galactic cosmic rays (GCRs) is modeled as well. During the SEP event of 23–24 August (Figure 7b), ionization at low altitudes (below the red line) is mostly due to solar protons, indicated by the solid line contours of ion pair production rate of 10^8 m^{-3} s^{-1}. The effect of GCRs is seen, for example, on 20 August 2005 in ionization between 20 and 40 km altitudes, indicated by the dashed line contours of the production rate of 10^6 m^{-3} s^{-1}. Around 25 August at the peak of geomagnetic storm, the low-altitude ionization is missing (Forbush-like decrease). Similar effect is observed on 8–10 November 2004 (Figure 7a). For both the November 2004 (Figure 7a) and August 2005 (Figure 7b) events, the electron contribution reaches up to ~90% during the main phase from about 70 km altitude and up. Exceptions are for 22–23 August 2005 (234–235 day of year (DOYs)) and a part of 8 November 2004 (313 DOY), which correspond to peaks of the SEP events, and results in ionization dominated by protons.

This characteristic altitude cutoff changes during the event, which is especially clear for the August 2005 event. The SEP flux starts to increase on 22 August and reaches a maximum on 23 to 25 August (Paper I). The proton ionization peaks on 23 August at ~10^9 ion pair/(m^3 s) and at 60–90 km, while the electron contribution is negligible at these altitudes (Figure 7b). One day later, on 24 August (236 DOY) the proton ionization switches to lower energies and shifts upward into the normally electron-dominated altitude. This is the day when the geomagnetic storm main phase and then a recovery phase occur (see Figure 2b), causing magnetospheric electron precipitation. Ionization due to electrons peaks at ~115 km reaching 10^{10} ion pair/(m^3 s) and dominates the total ionization rate. Lower altitudes (70–100 km) are now dominated by high-energy electrons, reaching similar ionization levels at the upper proton peak and contributing 60–90%. Contribution from precipitating electrons drops sharply below ~70 km, where auroral electron contribution is negligible and modeled ionization is due to bremsstrahlung only.

For the November 2004 event solar protons dominate on 8 November only with ~10^9 ion pair/(m^3 s). Hereafter, proton-produced ionization maxima coincide with electron-produced maxima at 70–120 km. In both cases the electron contribution reaches more than 90% at 90 km altitude. The geomagnetic storm main phase onset is on 8 November (see Figure 2a) and electron precipitation is expected throughout 11 November. Note that Figures 5 and 6 and the corresponding analysis in sections 3.2 and 3.3 were pertinent to the nighttime only.

3.6. Estimates of Peak Zonal OH Production and Comparison With Observations

We provide an estimate of the peak zonal OH production in the high-latitude nighttime mesosphere during SEP events based on modeled proton and electron ionization rates and compare with observations. According to MLS observations, a peak in the nightly averaged zonal OH density of ~$3.5 \cdot 10^{12}$ m^{-3} during the November 2004 event occurred in the Northern Hemisphere high-latitude bin at a pressure level of ~0.01 hPa (~80 km) at the beginning of 9 November (Figure 1a). The corresponding modeled zonal ionization rate (at the same day and around the same pressure level) due to precipitating protons is ~$7 \cdot 10^8$ m^{-3} s^{-1} (see Figure 5a). From Figure 6a, the ionization due to electrons for this event is smaller, with at most ~10^8 m^{-3} s^{-1} (see Figure 6a). Given a 2 h modeling time step, the ion pair production due to precipitating particles can be estimated as ~$3 \cdot 10^{12}$ m^{-3}. *Solomon et al*. [1981] analyzed odd hydrogen production due to particle precipitation in the mesosphere and suggested that, in general, below 60 km altitude (about 0.1 hPa) approximately 1.8 odd hydrogen molecules are created per ion pair. They noted that the ratio (the number of HO_x molecules per ion pair) is somewhat less than 2 for higher altitudes. *Verronen and Lehmann* [2013] performed a comprehensive modeling study of ion chemistry during proton events and demonstrated that the ratio is highly variable at nighttime mesospheric altitudes depending on season, ionization level, and latitude. Their results (see their Figure 5) indicate that the ratio can be as low as 0.5 at ~80 km altitude with the *Solomon et al*. [1981] estimate as the upper limit. For a more conservative estimate of peak hydroxyl density we use modeled production factors provided by *Verronen and Lehmann* [2013]. The estimated values are from 1.58 to 1.73 for the number of odd hydrogen molecules created per ion pair at 80 km altitude and for the production rate range of 10^8 to 10^9 m^{-3} s^{-1} of combined hydroxyl and atomic hydrogen in high-latitude Northern Hemisphere for October under the nighttime condition of SZA $>$ 100° (their tables A17 and A19). Thus, for the peak OH production during the November event we estimate ~$4.7 \cdot 10^{12}$ m^{-3} to $5.2 \cdot 10^{12}$ m^{-3} from the modeled ionization rates. This value is higher than the observations. Some of that difference could be explained by the fact that we compare our estimates based on peak modeled values defined every 2 h with nightly averaged observations, which provide lower values for the densities. *Verronen and Lehmann* [2013] estimate the production factors in polar winter hemispheres from 55° to 75°. In this paper the observed OH production peaks occurred in November and between 60° and 70° (Figure 1a); thus, specific production factors for this case could be slightly different from the modeled values of *Verronen and Lehmann* [2013].

Precipitating electrons provided the major contribution to ionization, both in high-latitude Northern and Southern Hemispheres on 10 November 2004 during the recovery phase of the geomagnetic storm (Figure 6a and 6d). Peak zonal ionization rate at 0.01 hPa pressure level is ~$7 \cdot 10^9$ m^{-3} s^{-1} which gives an estimate of ~$7 \cdot 10^{12}$ m^{-3} in ion pairs and of ~10^{13} m^{-3} in OH zonal density. Nightly averaged zonal density from the MLS measurements is ~$4 \cdot 10^{12}$ m^{-3} (Figure 1d) which is lower.

For the August 2005 event, the observed peak nightly averaged zonal OH production of ~$4 \cdot 10^{12}\,m^{-3}$ was reached on 24 August at ~0.02 hPa pressure level (Figure 1e). The corresponding modeled zonal ion production of ~$10^{9}\,m^{-3}\,s^{-1}$ is due to precipitating protons (Figure 5e), and ~$10^{8}\,m^{-3}\,s^{-1}$ is due to precipitating electrons (Figure 6e). Since *Verronen and Lehmann* [2013] estimated production factors for January and October only, we used a general range of production factor values from 0.5 to 1.8 following *Solomon et al.* [1981]. Ionization could cause ~$2 \cdot 10^{12}\,m^{-3}$ to $7 \cdot 10^{12}\,m^{-3}$ zonal OH density production. These simple estimates agree with the MLS observations.

4. Discussion and Conclusions

In the paper we analyzed contributions from solar protons and magnetospheric electrons to observed nighttime averaged zonal OH density enhancements based on MLS measurements in the atmospheric pressure level range from 0.001 hPa to 0.2 hPa (mesospheric altitudes) during two SEP events and concomitant geomagnetic storms. We focused on the middle (±50°) to high geographic latitudes (±70°). To our knowledge this is the first study of nighttime hydroxyl enhancements due to a combined effect of solar protons and magnetospheric electrons. Based on simple estimates, we confirmed a direct relationship between precipitating particle fluxes, ionization rates due to both protons and electrons, and nighttime OH density enhancements. We summarize our main results as follows:

1. AIMOS model was used to estimate atmospheric ionization rates due to precipitating energetic particles. Solar proton fluxes measured by GOES and energetic magnetospheric electron fluxes measured by POES were combined and processed for input into the model. We utilized an improved version 1.6 of AIMOS which provided more realistic electron ionization rates between 70 km and 90 km.
2. From the modeled ionization rates at the 2 h local time window around average nighttime Aura/MLS measurements, local peak zonal OH density production estimates are ~$10^{13}\,m^{-3}$ to $5.4 \cdot 10^{12}\,m^{-3}$ for the November event (dominated by electrons) and ~$2 \cdot 10^{12}\,m^{-3}$ to $7 \cdot 10^{12}\,m^{-3}$ for the August event (dominated by protons). Our modeling results are in agreement with the Aura/MLS observations, however, somewhat higher, especially for the November event (Figure 1). Note that we compare nightly averaged values to estimated peak values from modeled ionization rates with 2 hour data cadence around the average local time. Averaged values are expected to be lower than or equal to the peak values occurring during a day, which could represent the lower end estimate of the actual OH densities.
3. AIMOS modeling shows that both SEPs and precipitating electrons contribute (often simultaneously) to the total ionization of the middle atmosphere during SEP events and strong geomagnetic storms which causes enhancements of nighttime hydroxyl, but their relative contributions change throughout the time intervals. The electron contribution could reach ~90% at the 70–120 km altitude range during the recovery phase of a geomagnetic storm. The relative contribution depends, of course, on strength and duration of SEP event and concomitant geomagnetic storm and their relative timing.

The new feature of this approach is to model mesospheric ionization and hydroxyl enhancement due to both solar proton and magnetospheric electrons. Another important feature is to utilize combined in situ satellite measurements of particle spectra. Our result underlines the importance of a combined solar proton and magnetospheric electron precipitation for hydroxyl abundance and the middle atmosphere chemistry, in general.

We suggest the following timeline for the physical causes of mesospheric ionization for these two events. First, a solar flare(s) produces high-energy solar protons and initiates a SEP event. Some fraction of the solar wind population (possibly including particles of flare origin [*Verkhoglyadova et al.*, 2010]) is accelerated at a shock driven by a CME(s). Since particles are accelerated continuously at a traveling shock, the corresponding SEP fluxes at Earth's orbit could stay elevated for days and cause mesosphere ionization. If a CME causes a geomagnetic storm, this typically leads to the acceleration of radiation belt electrons [e.g., *Horne et al.*, 2005]. These electrons precipitate at high latitude to the subauroral night and dawn atmosphere from the end of the main storm phase into the recovery storm phase [see, e.g., *Gonzalez et al.*, 1994; *Schunk and Nagy*, 2009]. Thus, electron-caused atmospheric ionization can be delayed compared to solar proton-caused ionization [see also *Rodger et al.*, 2010].

Realistic event-based modeling of atmospheric ionization rates with inputs from actual in situ precipitating particle measurements can provide a causative link between SEP and precipitating electron fluxes, nighttime

OH density dynamics, and its global distribution. Both energetic particle populations are important for understanding ionization-driven changes in mesospheric composition and potential short-time mesospheric tertiary O_3 destruction.

Acknowledgments
Portions of this work were done at the Jet Propulsion Laboratory, California Institute of Technology, under a contract with the National Aeronautics and Space Administration. Government Sponsorship acknowledged. S.W. acknowledges the support of the NASA Aura Science Team program. We are thankful to the NOAA Space Weather Prediction Center for providing POES and GOES particle data. The AIMOS model can be accessed at http://aimos.physik.uos.de. The authors acknowledge the use of OMNI database supported by NASA GSFC (at http://satdat.ngdc.noaa.gov/sem/goes/data/new_avg/ and http://omniweb.gsfc.nasa.gov/form/omni_min.html). MLS data are provided through http://mls.jpl.nasa.gov/.

References

Agostinelli, S., et al. (2003), GEANT4: A simulation toolkit, *Nucl. Instrum. Methods Phys. Res., Sect. A*, *506*, 250–303.
Andersson, M. E., P. T. Verronen, S. Wang, C. J. Rodger, M. A. Clilverd, and B. R. Carson (2012), Precipitating radiation belt electrons and enhancements of mesospheric hydroxyl during 2004–2009, *J. Geophys. Res.*, *117*, D09304, doi:10.1029/2011JD017246.
Cane, H. V., D. V. Reames, and T. T. von Rosenvinge (1988), The role of interplanetary shocks in the longitude distribution of solar energetic particles, *J. Geophys. Res.*, *93*, 9555–9567, doi:10.1029/JA093iA09p09555.
Damiani, A., M. Storini, M. Laurenza, and C. Rafanelli (2008), Solar particle effects on minor components of the polar atmosphere, *Ann. Geophys.*, *26*, 361–370.
Damiani, A., M. Storini, C. Rafanelli, and P. Diego (2010), The hydroxyl radical as an indicator of SEP fluxes in the high-latitude terrestrial atmosphere, *Adv. Space Res.*, *46*, 1225–1235.
Funke, B., et al. (2011), Composition changes after the "Halloween" solar proton event: the High Energy Particle Precipitation in the Atmosphere (HEPPA) model versus MIPAS data intercomparison study, *Atmos. Chem. Phys.*, *11*, 9089, doi:10.5194/acp-11-9089-2011.
Gonzalez, W. D., J. A. Joselyn, Y. Kamide, H. W. Kroehl, G. Rostoker, B. T. Tsurutani, and V. M. Vasyliunas (1994), What is a geomagnetic storm?, *J. Geophys. Res.*, *99*, 5771–5792, doi:10.1029/93JA02867.
Horne, R. B., et al. (2005), Wave acceleration of electrons in the Van Allen radiation belts, *Nature*, *437*, 227–230, doi:10.1038/nature03939.
Iyemori, T. (1990), Storm-time magnetospheric currents inferred from midlatitude geomagnetic field variations, *J. Geomagn. Geoelectr.*, *42*, 1249–1265.
Jackman, C. H., M. T. DeLand, G. J. Labow, E. L. Fleming, D. K. Weisenstein, M. K. W. Ko, M. Sinnhuber, and J. M. Russell (2005), Neutral atmospheric influences of the solar proton events in October–November 2003, *J. Geophys. Res.*, *110*, A09S27, doi:10.1029/2004JA010888.
Jackman, C. H., M. T. Deland, G. J. Labow, E. L. Fleming, and M. López-Puertas (2006), Satellite measurements of middle atmospheric impacts by solar proton events in solar cycle 23, *Space Sci. Rev.*, *125*, 381–391.
Jackman, C. H., et al. (2011), Northern Hemisphere atmospheric influence of the solar proton events and ground level enhancement in January 2005, *Atmos. Chem. Phys.*, *11*, 6153–6166, doi:10.5194/acp-11-6153-2011.
Kallenrode, M.-B. (2003), Current views on impulsive and gradual solar energetic particle events, *J. Phys. G: Nucl. Part. Phys.*, *29*, 965–981.
Leske, R. A., R. A. Mewaldt, E. C. Stone, and T. T. von Rosenvinge (2001), Observations of geomagnetic cut-off variations during solar energetic events and implications for the radiation environment at the Space Station, *J. Geophys. Res.*, *106*, 30,011–30,022, doi:10.1029/2000JA000212.
Livesey, N. J., V. W. Snyder, W. G. Read, and P. A. Wagner (2006), Retrieval algorithms for the EOS Microwave Limb Sounder (MLS), *IEEE Trans. Geosci. Remote Sens.*, *44*(5), 1144–1155.
Livesey, N. J., et al. (2015), Earth Observing System (EOS) Microwave Limb Sounder (MLS) Version 4.2x Level 2 data quality and description document, Report JPL D-33509, Jet Propulsion Laboratory, California Institute of Technology, Pasadena, Calif.
Marsh, D., A. Smith, G. Brasseur, M. Kaufmann, and K. Grossmann (2001), The existence of a tertiary ozone maximum in the high-latitude middle mesosphere, *Geophys. Res. Lett.*, *28*(24), 4531–4534, doi:10.1029/2001GL013791.
Pickett, H. M., B. J. Drouin, T. Canty, L. J. Kovalenko, R. J. Salawitch, N. J. Livesey, W. G. Read, J. W. Waters, K. W. Jucks, and W. A. Traub (2006a), Validation of Aura MLS HO_x measurements with remote-sensing balloon instruments, *Geophys. Res. Lett.*, *33*, L01808, doi:10.1029/2005GL024048.
Pickett, H. M., W. G. Read, K. K. Lee, and Y. L. Yung (2006b), Observations of night OH in the mesosphere, *Geophys. Res. Lett.*, *33*, L19808, doi:10.1029/2006GL026910.
Rodger, C. J., M. A. Clilverd, J. C. Green, and M. M. Lam (2010), Use of POES SEM-2 observations to examine radiation belt dynamics and energetic electron precipitation into the atmosphere, *J. Geophys. Res.*, *115*, A04202, doi:10.1029/2008JA014023.
Schmidt, H., G. P. Brasseur, M. Charron, E. Manzini, M. A. Giorgetta, and T. Diehl (2006), The HAMMONIA chemistry climate model: Sensitivity of the mesopause region to the 11-year solar cycle and CO_2 doubling, *J. Clim.*, *19*, 3902–3931.
Schunk, R. W., and A. F. Nagy (2009), *Ionospheres: Physics, Plasma Physics, and Chemistry*, 2nd ed., Cambridge Univ. Press, Cambridge, U. K.
Seppälä, A., P. T. Verronen, V. F. Sofieva, J. Tamminen, E. Kyrölä, C. J. Rodger, and M. A. Clilverd (2006), Destruction of the tertiary ozone maximum during a solar proton event, *Geophys. Res. Lett.*, *33*, L07804, doi:10.1029/2005GL025571.
Sofieva, V. F., et al. (2009), Spatio-temporal observations of the tertiary ozone maximum, *Atmos. Chem. Phys.*, *9*, 4439–4445.
Solomon, S., D. W. Rusch, J.-C. Gérard, G. C. Reid, and P. J. Crutzen (1981), The effect of particle precipitation events on the neutral and ion chemistry of the middle atmosphere: II. Odd hydrogen, *Planet. Space Sci.*, *29*(8), 885–893.
Solomon, S., D. W. Rusch, R. J. Thomas, and R. S. Eckman (1983), Comparison of mesospheric ozone abundance measured by the Solar Mesosphere Explorer and model calculations, *Geophys. Res. Lett.*, *10*, 249–252, doi:10.1029/GL010i004p00249.
Turunen, E., P. T. Verronen, A. Seppälä, C. J. Rodger, M. A. Clilverd, J. Tamminen, C.-F. Enell, and T. Ulich (2009), Impact of different energies of precipitating particles on NO_x generation in the middle and upper atmosphere during geomagnetic storms, *J. Atmos. Sol. Terr. Phys.*, *71*, 1176–1189.
Verkhoglyadova, O. P., G. Li, G. P. Zank, Q. Hu, C. M. S. Cohen, R. A. Mewaldt, G. M. Mason, D. K. Haggerty, T. T. von Rosenvinge, and M. D. Looper (2010), Understanding large SEP events with the PATH code: Modeling of the 13 December 2006 SEP event, *J. Geophys. Res.*, *115*, A12103, doi:10.1029/2010JA015615.
Verkhoglyadova, O. P., G. P. Zank, and G. Li (2014), A theoretical perspective on particle acceleration by interplanetary shocks and the Solar Energetic Particle problem, *Phys. Rep.*, doi:10.1016/j.physrep.2014.10.004.
Verkhoglyadova, O. P., S. Wang, M. G. Mlynczak, L. A. Hunt, and G. P. Zank (2015), Effects of two large solar energetic particle events on middle atmosphere nighttime odd hydrogen and ozone content: Aura/MLS and TIMED/SABER measurements, *J. Geophys. Res. Space Physics*, *120*, 12–29, doi:10.1002/2014JA020609.
Verronen, P. T., and R. Lehmann (2013), Analysis and parameterisation of ionic reactions affecting middle atmospheric HO_x and NO_y during solar proton events, *Ann. Geophys.*, *31*, 909–956, doi:10.5194/angeo-31-909-2013.
Verronen, P. T., A. Seppala, E. Kyrola, J. Tamminen, H. M. Pickett, and E. Turunen (2006), Production of odd hydrogen in the mesosphere during the January 2005 solar proton event, *Geophys. Res. Lett.*, *33*, L24811, doi:10.1029/2006GL028115.

Verronen, P. T., C. J. Rodger, M. A. Clilverd, H. M. Pickett, and E. Turunen (2007), Latitudinal extent of the January 2005 solar proton event in the Northern Hemisphere from satellite observations of hydroxyl, *Ann. Geophys.*, *25*, 2203–2215.

Verronen, P. T., C. J. Rodger, M. A. Clilverd, and S. Wang (2011), First evidence of mesospheric hydroxyl response to electron precipitation from the radiation belts, *J. Geophys. Res.*, *116*, D07307, doi:10.1029/2010JD014965.

Verronen, P. T., M. E. Andersson, C. J. Rodger, M. A. Clilverd, S. Wang, and E. Turunen (2013), Comparison of modeled and observed effects of radiation belt electron precipitation on mesospheric hydroxyl and ozone, *J. Geophys. Res. Atmos.*, *118*, 11,419–11,428, doi:10.1002/jgrd.50845.

Verronen, P. T., M. E. Andersson, A. Kero, C.-F. Enell, J. M. Wissing, E. R. Talaat, K. Kauriste, M. Palmroth, T. E. Sarris, and E. Armandillo (2015), Contribution of proton and electron precipitation to the observed electron concentration in October–November 2003 and September 2005, *Ann. Geophys.*, *33*, 381–394, doi:10.5194/angeo-33-381-2015.

Waters, J. W., et al. (2006), The Earth Observing System Microwave Limb Sounder (EOS MLS) on the Aura satellite, *IEEE Trans. Geosci. Remote Sens.*, *44*, 1075–1092.

Winkler, H., M. Sinnhuber, J. Notholt, M.-B. Kallenrode, F. Steinhilber, J. Vogt, B. Zieger, K.-H. Glassmeier, and A. Stadelmann (2008), Modeling impacts of geomagnetic field variations on middle atmospheric ozone responses to solar proton events on long timescales, *J. Geophys. Res.*, *113*, D02302, doi:10.1029/2007JD008574.

Wissing, J. M., and M.-B. Kallenrode (2009), Atmospheric Ionization Module Osnabrück (AIMOS): A 3-D model to determine atmospheric ionization by energetic charged particles from different populations, *J. Geophys. Res.*, *114*, A06104, doi:10.1029/2008JA013884.

Wissing, J. M., J. P. Bornebusch, and M.-B. Kallenrode (2008), Variation of energetic particle precipitation with local magnetic time, *Adv. Space Res.*, *41*, 1274–1278.

Zank, G. P., G. Li, and O. P. Verkhoglyadova (2007), Particle acceleration at interplanetary shocks, *Space Sci. Rev.*, *130*, 255–272, doi:10.1007/s11214-007-9214-2.